Simulating the Proton Transfer in Gramicidin A by a Sequential Dynamical Monte Carlo Method

Mirco S. Till, Timm Essigke, Torsten Becker,* and G. Matthias Ullmann*

Structural Biology/Bioinformatics, University of Bayreuth, Universitätsstr. 30, BGI, 95447 Bayreuth, Germany

Received: February 19, 2008; Revised Manuscript Received: June 3, 2008

The large interest in long-range proton transfer in biomolecules is triggered by its importance for many biochemical processes such as biological energy transduction and drug detoxification. Since long-range proton transfer occurs on a microsecond time scale, simulating this process on a molecular level is still a challenging task and not possible with standard simulation methods. In general, the dynamics of a reactive system can be described by a master equation. A natural way to describe long-range charge transfer in biomolecules is to decompose the process into elementary steps which are transitions between microstates. Each microstate has a defined protonation pattern. Although such a master equation can in principle be solved analytically, it is often too demanding to solve this equation because of the large number of microstates. In this paper, we describe a new method which solves the master equation by a sequential dynamical Monte Carlo algorithm. Starting from one microstate, the evolution of the system is simulated as a stochastic process. The energetic parameters required for these simulations are determined by continuum electrostatic calculations. We apply this method to simulate the proton transfer through gramicidin A, a transmembrane proton channel, in dependence on the applied membrane potential and the pH value of the solution. As elementary steps in our reaction, we consider proton uptake and release, proton transfer along a hydrogen bond, and rotations of water molecules that constitute a proton wire through the channel. A simulation of 8 μs length took about 5 min on an Intel Pentium 4 CPU with 3.2 GHz. We obtained good agreement with experimental data for the proton flux through gramicidin A over a wide range of pH values and membrane potentials. We find that proton desolvation as well as water rotations are equally important for the proton transfer through gramicidin A at physiological membrane potentials. Our method allows to simulate long-range charge transfer in biological systems at time scales, which are not accessible by other methods.

Introduction

Long range proton transfer (LRPT) plays a major role in many biochemical processes.[1] Among them, biological energy transducing reactions such as cellular respiration, photosynthesis, and denitrification are of central importance for life. Although LRPT has been investigated extensively both experimentally and theoretically, the mechanism of these reactions is still not fully understood. One often discussed scenario is the so-called Grotthuss mechanism.[2,3] This mechanism assumes that the proton transfer reaction occurs in an already existing hydrogen bonded network. A subsequent rotation of the hydrogen bond partners restores the original network. In the Grotthuss mechanism, it is assumed that the rearrangement of the hydrogen bonded network is rate limiting for the LRPT. The actual transfer through the hydrogen bonded network is considered to be fast. Another proposed mechanism considers the energy barrier for transferring the proton through the hydrogen bonded network as rate limiting.[4] The rearrangement of the hydrogen bond pattern occurs during the LRPT and is thus not rate limiting.

To simulate LRPT in solution and in biological molecules, several approaches were developed. Many theoretical studies at different levels of approximation led to a detailed view of proton transfer reactions.[4−13] However, simulating the dynamics of LRPT processes in proteins still remains challenging. Two problems govern the simulation of LRPT processes. First, breaking of covalent bonds, which is typically addressed by quantum chemical methods, is necessary for proton transfer. Second, proton transfer processes across a cellular membrane occur on the microsecond time scale, which can not be simulated with current QM/MM methods.

The aim of the present work is to develop a general method for simulating LRPT in biomolecules. The approach that we are following is based on the master equation.[14,15] The elementary steps of the overall reaction are proton transfer and structural changes of the hydrogen bonded network. Since the number of possible states is rather large, we use a dynamical Monte Carlo (DMC) approach to solve the master equation.[16,17] In contrast to standard Metropolis Monte Carlo, DMC allows to simulate the kinetics of a reaction system.

We applied our DMC approach, to study the LRPT through gramicidin A (gA). This well-studied system consist of a head-to-head dimer of two helical peptides spanning the membrane.[18−20] The channel, which is formed in the center of the peptide, is filled by a file of water molecules.[4,21,22] Gramicidin A functions as an antibiotic exerting its activity by increasing the cation permeability of the target plasma membrane. Besides water and monovalent cations, also protons can pass the channel. While water molecules and cations diffuse through the channel, protons are transferred along a file of water molecules. This proton transfer across the membrane was measured experimentally in dependence on the pH value and the membrane potential.[23−26]

In this article, we describe a new DMC algorithm to simulate charge transfer in biomolecules. We discuss the theoretical

* Corresponding authors. E-mail: Matthias.Ullmann@uni-bayreuth.de (G.M.U.); Torsten.Becker@uni-bayreuth.de (T.B.). Fax: +49-921-55-3071.

10.1021/jp801477b CCC: $40.75 © 2008 American Chemical Society
Published on Web 09/30/2008

background and the implementation of the method. The method is applied to study the LRPT in gA for which we compare our results to experimental data. Due to the efficient Monte Carlo sampling, large molecular systems can be simulated over time ranges of biological interest. This approach will allow to investigate the underlying mechanism of biological charge transfer systems such as for example the photosynthetic reaction center, cytochrome *c* oxidase, and cytochrome bc_1.

Theory

Microstate Description. Biological charge transfer can be described as transitions between microstates of a system.[14,15,27−29] A microstate of a proton transfer system can be represented as an *N*-dimensional vector $\vec{x} = (x_1,..., x_i,..., x_N)$, where *N* is the number of protonatable sites of the system; x_i specifies the instance of site *i*, i.e., a combined representation of its protonation and rotameric form. Thus, assuming *p* possible instances x_i, there are in total $M = p^N$ possible microstates for the system. To keep the notation concise, microstates will be numbered by the Greek letters ν and μ, while we will use the roman letters *i* and *j* as site indices.

The standard energy for a given microstate $\vec{x}_\nu$ (i.e., the electrochemical potential of all ligands is zero) can be calculated by[30,31]

$$G_\nu^\circ = \sum_{i=1}^{N} (G_{\text{intr}}(x_i) + G_\Phi(x_i)) + \frac{1}{2}\sum_{i=1}^{N}\sum_{j=1}^{N} W(x_i, x_j) \qquad (1)$$

$G_{\text{intr}}(x_i)$ is the so-called intrinsic energy of the instance x_i, $G_\Phi(x_i)$ denotes the instance-specific energy contribution due to the membrane potential, and $W(x_i, x_j)$ takes into account the interactions between pairs of instances of different sites. If the electrochemical potential of the ligands is different from zero, the energy of the microstate differs from the standard energy. If we consider for simplicity that only protons can bind, the energy of the microstate ν at a given electrochemical potential $\bar{\mu}$ is given by

$$G_\nu = G_\nu^\circ - n_\nu \bar{\mu} \qquad (2)$$

where n_ν is the number of protons bound in microstate ν.

Equilibrium properties of a physical system are completely determined by the energies of its states. The equilibrium probability of a single state is given by

$$P_\nu^{\text{eq}} = \frac{e^{-\beta G_\nu}}{Z} \qquad (3)$$

with $\beta = 1/RT$ where *R* is the gas constant and *T* is the absolute temperature. *Z* is the partition function of the system.

$$Z = \sum_{\nu=1}^{M} e^{-\beta G_\nu} \qquad (4)$$

The sum runs over all *M* possible microstates. Macroscopic properties of the system can be obtained by summing up the individual contributions of all states. For example, the average number of bound protons is given by

$$\langle n \rangle = \sum_{\nu=1}^{M} n_\nu P_\nu^{\text{eq}} \qquad (5)$$

where n_ν denotes the number of bound protons in the microstate ν. For small systems, this sum can be evaluated explicitly. For larger systems, Monte Carlo techniques can be invoked to determine these probabilities.

Time Evolution of the System. The time evolution of the above-defined system can be described by a master equation

$$\frac{d}{dt} P_\nu(t) = \sum_{\mu=1}^{M} k_{\nu\mu} P_\mu(t) - \sum_{\mu=1}^{M} k_{\mu\nu} P_\nu(t) \qquad (6)$$

where $P_\nu(t)$ denotes the probability that the system is in state ν at time *t*, $k_{\nu\mu}$ denotes the probability per unit time that the system will change its state from μ to ν. The summation runs over all possible states μ. In principle, the time evolution of such a system can be solved analytically.[15] In the microstate description applied in this work, the number of states might become very large, so that solving eq 6 directly is computationally prohibited. To overcome this problem, stochastic methods, which have been developed to deal with complex kinetic systems, can be applied.[16,32,33] In such methods, the system—for example a chemical reaction system—is described by a discrete amount of particles of each species present. Transition rates are calculated for all possible reactions depending on the current number of particles. Although these stochastic methods are efficient in solving eq 6, they still require the calculation and the storage of all possible microstates and rate constants for all possible transitions. Such an approach would overstretch nowadays computational resources for a microstate description even of a biological molecule of moderate size.

In this paper, we introduce a DMC method which allows to solve eq 6 using affordable computational resources. The underlying idea is that although there is an overwhelming number of possible microstates, most of these states will never be populated, since they are energetically too unfavorable. However, deciding in advance, which microstates are important for the reaction dynamics of a system, could introduce a bias with consequences which are hard to estimate. To avoid this bias, we follow the time evolution of a single initial microstate and let our algorithm decide, which microstates will be populated in the course of the simulation. The time evolution of a given microstate is simulated by the Gillespie algorithm.[16] In order to get statistically significant results, the simulations need to be repeated several times. We call this variant of the DMC method sequential DMC. For a small test system with five sites,[15] we test the correctness of the implementation of our sequential DMC algorithm by comparing the analytically obtained kinetics with those calculated by the sequential DMC method (data not shown).

Figure 1 shows a flowchart of our sequential DMC algorithm which is based on the Gillespie algorithm. Starting from an initial microstate, rate constants are calculated for all events possible. An event is a transition between microstates. In our simulation, only one elementary step (proton uptake, proton release, proton transfers through a hydrogen bond, or rotation of a water molecule) is allowed in one event. The number of possible events for a given microstate is typically small and maximally on the order of N^2p, where *N* is the number of sites and *p* the number of instances per site. Thus, the total number of all possible events in the system (which is maximally in the order of p^{2N}) is drastically reduced. Given the rate constants of the possible events starting from the given microstate, the algorithm chooses the next event *m* according to the following criterion [16,17]

$$\sum_{l=1}^{m-1} k_l \le \rho_1 K < \sum_{l=1}^{m} k_l \tag{7}$$

$$K = \sum_{l=1}^{L} k_l \tag{8}$$

K is the sum of the rate constants k_l of all L possible events for the given microstate; ρ_1 is a random number between 0 and 1. The rate constant k_l is equivalent to one of the rate constants in eq 6 and is a measure of the probability that event l happens during the next time step. To adequately represent the kinetic behavior of the system, it has to be ensured that the events are chosen in accordance with their respective probability. Thus, if a rate constant k_r is twice as large as a rate constant k_s, event r should on average be chosen twice as often as event s. This behavior is facilitated by eq 7. In the given example, k_r contributes twice as much as k_s to the sum K and, thus, the probability that event r fulfills eq 7 is twice as large as that for event s.

The time Δt that elapsed during the Monte Carlo step is given by

$$\Delta t = \frac{1}{K} \ln\left[\frac{1}{\rho_2}\right] \tag{9}$$

which is a standard way to draw a random number Δt from an exponential distribution given a uniformly distributed random number ρ_2 between 0 and 1. Thus, eq 9 is equivalent to the statement that the probability of any event to happen within time Δt is given by $\exp(-K\Delta t)$. In summary, the criteria in eqs 7 and 9 ensure that.

(i) all events are chosen according to their respective probability and

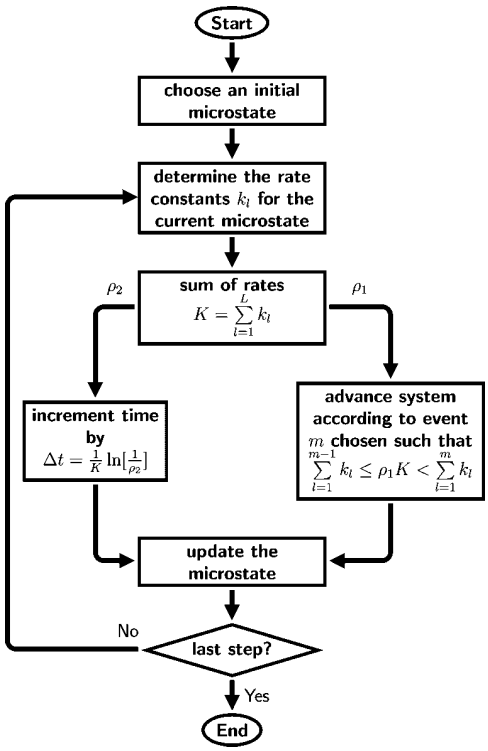

Figure 1. Flowchart of the sequential DMC algorithm. Starting from a microstate, rate constants for all possible events are calculated. The time increment and the reaction to take place are chosen based on the calculated rate constants and two random numbers (ρ_1 and ρ_2) between 0 and 1.

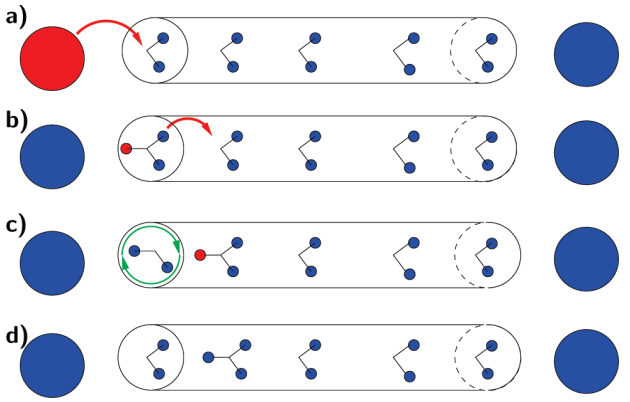

Figure 2. Different kinds of possible reactions included in the sequential DMC algorithm. (a) Representation of the uptake of a proton. (b) Proton transfer between neighboring water molecules. (c) Rotation of the first water molecule. (d) State of the channel after all three elementary reaction steps.

(ii) the average time evolution of the system follows a master equation.

Application of the described algorithm provides a trajectory, i.e., a succession of microstates with accompanying time information. Comparison to experimental data can be made by averaging over several trajectories:

$$\langle B \rangle = \frac{1}{N_{\mathrm{Tr}}} \sum_{l=1}^{N_{\mathrm{Tr}}} B_l \tag{10}$$

where $\langle B \rangle$ is any given measurable quantity and B_l is its value for a given trajectory l, N_{Tr} is the number of trajectories. The flux F of protons through the channel, for example, is calculated as follows:

$$\langle F \rangle = \frac{1}{N_{\mathrm{Tr}}} \sum_{l=1}^{N_{\mathrm{Tr}}} F_l = \frac{1}{N_{\mathrm{Tr}}} \sum_{l=1}^{N_{\mathrm{Tr}}} \frac{f_l}{t_{\mathrm{Tr}}} \tag{11}$$

where t_{Tr} is the time elapsed in one trajectory and f_l is the number of the protons that are transferred from ectoplasm to cytoplasm in trajectory l.

Description of the Model System. The dimeric proton channel gA was chosen as a model system to test the DMC approach. The proton transfer through this channel occurs along a file of water molecules. In our simulation, the water molecules can rotate and protonate. Proton transfer can only occur between neighboring water molecules. Proton uptake and release takes place only at the water molecules at the two ends of the channel. The water molecules can assume different orientations: four for the protonated water molecule (H_3O^+) and six for the neutral water molecule (H_2O, see the section Water Representation in Computational Details). A rotation is the transition between different orientations of a water molecule; the protonation is not allowed to change during a rotation. Since our system contains eleven water molecules that can exist in ten different instances, the total number of different microstates is 10^{11}. In the simulation, only one elementary step (proton uptake, proton release, proton transfer, or rotation of a water molecule) is allowed in one Monte Carlo step. The model system and the possible reactions are schematically depicted in Figure 2.

Calculation of the Rate Constants. The rate constant $k_{\nu\mu}$ of the transition from state μ to state ν is calculated using an Arrhenius approach

$$k_{\nu\mu} = A_{\nu\mu} e^{-\beta G^{\ddagger}_{\nu\mu}} \tag{12}$$

The preexponential factor $A_{\nu\mu}$ was set to 10^{13} s^{-1}, which approximates the preexponential factor kT/h derived from

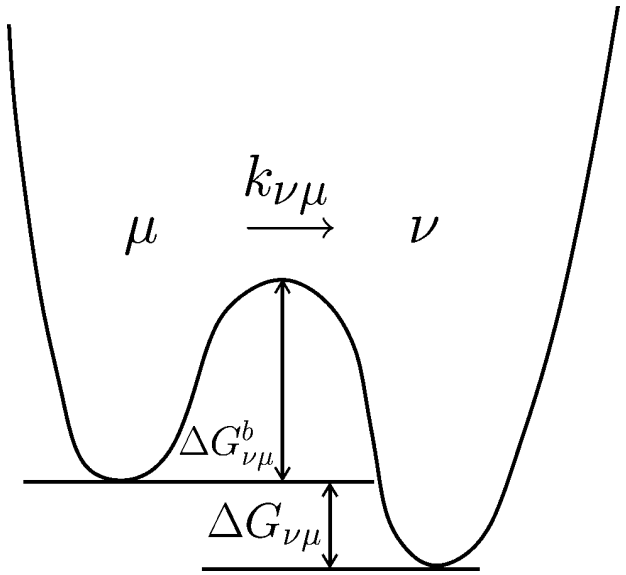

Figure 3. Energy profile of a reaction (proton uptake, proton release, proton transfer, or rotation of a water molecule) within our system. μ and ν are the microstates, $k_{\nu\mu}$ is the reaction rate constant for the reaction from μ to ν. $\Delta G^{b}_{\nu\mu}$ is the energy barrier, and $\Delta G_{\nu\mu}$ is the difference between the microstate energies of ν and μ.

transition state theory, where k is the Boltzmann constant, T is the temperature and h is Planck's constant. This preexponential factor $A_{\nu\mu}$ represents the maximal rate corresponding to an activationless transition. The activation energy $G^{\ddagger}_{\nu\mu}$ is given by

$$G^{\ddagger}_{\nu\mu} = \begin{cases} \Delta G_{\nu\mu} + \Delta G^{b}_{\nu\mu} & : \quad \Delta G_{\nu\mu} > 0 \\ \Delta G^{b}_{\nu\mu} & : \quad \Delta G_{\nu\mu} \le 0 \end{cases} \tag{13}$$

$\Delta G_{\nu\mu}$ is the energy difference between the microstates μ and ν. $\Delta G^{b}_{\nu\mu}$ is the energy barrier between the microstates μ and ν. The meaning of the symbols is illustrated in Figure 3. The way of obtaining energy barriers for the elementary reactions of our system is described in the following.

Proton Transfer Along a Hydrogen Bond. Proton transfer can only occur between a hydronium ion and a water molecule that form a hydrogen bond. Which pairs of molecules form a hydrogen bond can be determined based on geometric criteria: the O−O distance between these water molecules is less than 4 Å and the hydrogen atom of the donor molecule points toward the lone pair of the acceptor molecule. An angle criteria for an hydrogen bond is derived from the regular tetrahedron structure of the water molecules. Only hydrogen bonds with an hydrogen bond angle that deviates from 180° by less than 55° are considered. The energy difference between the reactant state and the product state is calculated from eq 1. The energy barrier for a proton transfer along a hydrogen bond in water is rather small.[10,34,35] Therefore, we set the energy barrier $G^{b}_{\nu\mu}$ for the proton transfer reaction to a fixed value of 0.5 kcal/mol in agreement with quantum chemical calculations.[10,34,35] With an average proton transfer rate constant of 3 ps^{-1} (taken from a simulation without membrane potential), we can estimate a transfer time of about 330 fs from our calculations which is in the same order of magnitude as proton transfer times determined from simulations of proton transfer in water.[36,37] The two calculations should result in comparable proton transfer rates, since the environment within the gA channel is similar to that in bulk water phase. In both cases, a water molecule forms several hydrogen bonds. In the gA channel, hydrogen bonds are formed with waters and the peptide backbone.

Proton Uptake and Release. The rate of proton uptake and release depends on the proton electrochemical potential $\bar{\mu}$ of the surrounding medium.

$$\bar{\mu} = -RT\ln(10)\mathrm{pH} + zF\phi \tag{14}$$

where R is the gas constant, T the absolute temperature, z is the charge of a proton, F is Faraday's constant, and ϕ is the membrane potential. The energy difference $\Delta G_{\nu\mu}$ between the product state ν and the reactant state μ is given by

$$\Delta G_{\nu\mu} = \Delta G^{\circ}_{\nu\mu} - \Delta G^{\circ}_{H_2O} - \lambda\bar{\mu} \tag{15}$$

where λ is -1 for proton release reactions and $+1$ for proton uptake reactions. $\Delta G^{\circ}_{H_2O}$ is the energy for protonating a water molecule in the bulk at standard conditions, which takes into account that the proton is taken up from or released to the bulk water. This value can be calculated from the pK_a value for the protonation of a water molecule and is 2.3 kcal/mol.

The energy barrier $\Delta G^{b}_{\nu\mu}$ for taking up a proton from the bulk water into the gA channel has two contributions. First, the energy barrier for transferring a proton in bulk water, which is at least 1.9 kcal/mol[3]. Second, the transfer of a proton from the bulk to the surface of the membrane, which was estimated to be about 2.7 kcal/mol.[38,39] These two contributions lead to a value of at least 4.6 kcal/mol for the energy barrier of the proton uptake and release, which is the value used in this study.

Rate Constants for Rotations of Molecules. The barrier of the rotation of a water or a hydronium molecule is assumed to depend on the number of hydrogen bonds that need to be broken to allow this rotation, no matter if these hydrogen bonds are formed again after the rotation. Hydrogen bonds are defined as explained above. The energy for breaking the hydrogen bonds determines the energy barrier $G^{b}_{\nu\mu}$. To calculate the energy for breaking a hydrogen bond, we apply an empirical formula (eq 16).[40] The energy barrier $G^{b}_{\nu\mu}$ is given by summing over the contribution of all H hydrogen bonds that need to be broken,

$$G^{b}_{\nu\mu} = \sum_{l=1}^{H} a e^{-cr_l} \tag{16}$$

where r_l is the O···H distance; a and c are empirical constants which have the values 6042 kcal/mol and 3.6 $Å^{-1}$, respectively. Equation 16 leads to hydrogen bond energies between 4.5 and 0.5 kcal/mol for H···O distances between 2 and 5 Å, respectively. The energy difference between the reactant state and the product state are again calculated from eq 1. In order to avoid barrierless rotation events, the minimum barrier is set to 1.0 kcal/mol. Woutersen et al.[41] measured the rotation rate of water molecules in bulk water by IR-spectroscopy. These authors found two rotation times for water molecules, 0.7 ps for weakly, and 13 ps for strongly hydrogen bonded water molecules. Since in our system water molecules have less hydrogen bonds than in liquid water, a rotation time of 1.1 ps, which we obtained from our simulations, is in good agreement with the experimental data.

Computational Details

Structure Preparation. Coordinates of gA are taken from the PDB (code 1jno).[42] A cube of dummy atoms (20 × 20 × 20 $Å^3$) with zero charge is placed around the structure to represent the lipid bilayer. Since the structure is determined by NMR, no positions for water molecules are available in the structure. To generate water positions, the system is placed in a water box. All water molecules overlapping with the system are deleted. A short steepest descent energy minimization (1000 steps)

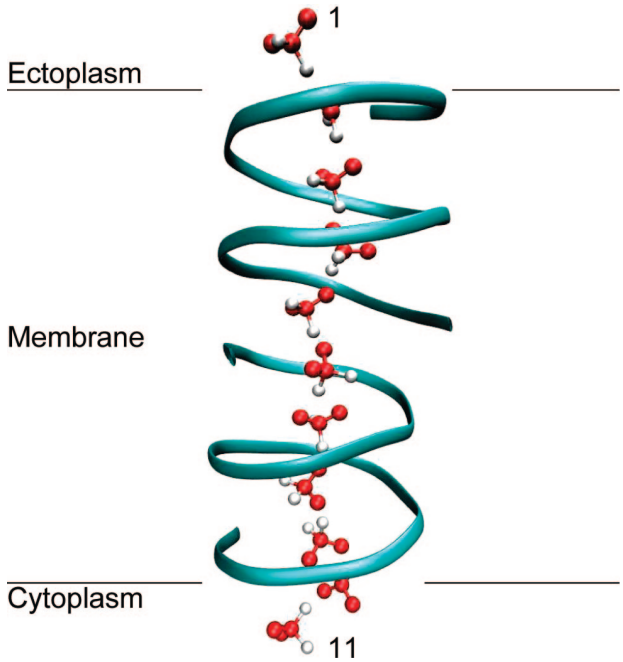

Figure 4. Gramicidin A system used in the simulation. The system contains eleven water molecules buried inside the gramicidin A membrane channel. The water model is depicted with the oxygen atom at the center and two lone pairs (red) and two hydrogen atoms (white).

followed by an adopted basis Newton−Raphson minimization (10 000 steps) is done using CHARMM.[43] Peptide heavy atoms and membrane atoms are kept fixed for both minimizations. In agreement with previous simulations,[4,21,22] we found nine water molecules in the channel. Two additional water molecules, one on each side of the channel, are selected to connect the water file within gA to the bulk solvent. These water molecules are in contact with the water molecules in the channel. The total number of water molecules thus amounts to eleven. Finally, the surrounding water box is removed and the eleven water molecules are replaced by our five-center water model (see next section). The resulting structure (see Figure 4) is used in all electrostatic calculations.

Water Representation. The incorporation of rotation events in our simulations requires an efficient way of calculating the contributions of the different rotameric forms of a water molecule to the microstate energy. For this purpose, we designed a symmetric water model based on a regular tetrahedron with five interaction centers, one at the center of the tetrahedron and the remaining four at each corner of the tetrahedron. The distance between the central and the four peripheral interaction centers is 0.95. The central interaction center represents the oxygen atom and the peripheral interaction centers represent either lone pairs or hydrogen atoms. The peripheral centers are permutated to sample all possible rotameric forms. No coordinates need to be changed, only atom labels and charges are assigned to already existing interaction centers. This water representation makes the calculation of state energies (eq 1) very efficient. Multipole-derived charges[44] for the possible protonation forms (H_2O and H_3O^+) are calculated using ADF.[45] For the H_2O molecule, the oxygen atom, the hydrogen atoms, and the lone pairs have a charge of −0.22, 0.21, and −0.10, respectively. For the H_3O^+ molecule, the respective atoms have a charge of 0.13, 0.32, and −0.09. Zundel ions were not considered explicitly, but geometries that correspond to Zundel ions where included in the simulation.

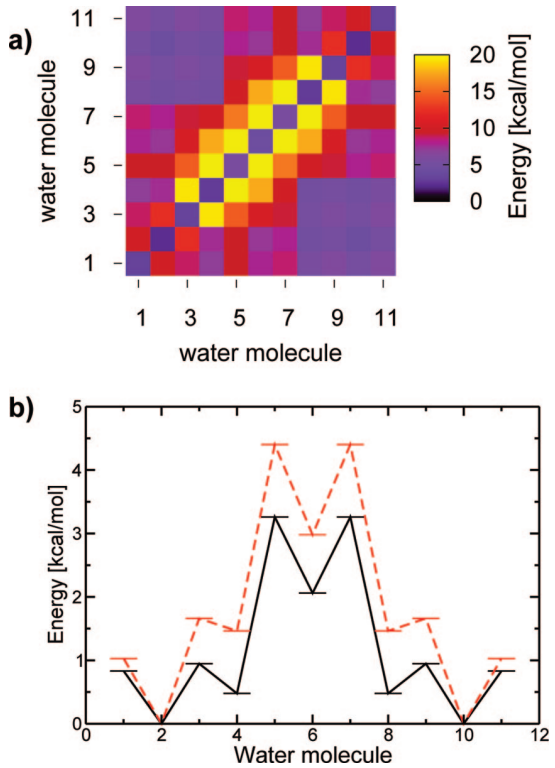

Figure 5. (a) Two dimensional potential of mean force for binding protons to the gA channel without membrane potential. The diagonal represents states with one proton bound. All other squares represent states with two protons bound, i.e., the entry (1,5) represents the state in which one proton is bound to water molecule 1 and the other proton to water molecule 5. The plot is symmetric, because entry (1,5) and entry (5,1) represent the same physical situation. (b) Energy profiles for the gA channel with exactly one proton inside the channel. The solid line depicts the potential of mean force. The dashed line is the minimum energy profile. For better comparison, both profiles are shifted with their minimum value to 0 kcal/mol.

Electrostatic Calculations. The energetic parameters in eq 1 ($G_{intr}(x_i)$, $G_\Phi(x_i)$, $W(x_i, x_j)$) are calculated from the solution of the Poisson−Boltzmann equation.[30,31] The intrinsic energies $G_{intr}(x_i)$ and the interaction energies $W(x_i, x_j)$ are obtained by using the MEAD package.[46] The dielectric constant for the protein and the membrane is set to 4 and the dielectric constant of the solvent is set to 80. The ionic strength is set to 0.1 M. The electrostatic potential is calculated by focusing using two grids of 81^3 grid points and a grid spacing of 1.0 and 0.25 Å. The first grid is centered on gA, and the second grid, on the water molecule of interest. Partial charges for the water molecules are taken from the ADF calculations as described before, partial charges for the peptide are taken from the CHARMM force field.[47] Energy contributions due to the membrane potential $G_\Phi(x_i)$[31] are calculated by the PBEQ module[48,49] of CHARMM[43] using the same settings as for the MEAD calculations. In order to account for the symmetry of gA, we symmetrized the energetic parameters in eq 1, i.e., we assigned the same energy parameters ($G_{intr}(x_i)$, $W(x_i, x_j)$) to symmetry related water molecules.

DMC Calculations. The time evolution of the system is simulated by calculating possible transitions between the microstates. A microstate is described by a vector with eleven elements, each element represents one water molecule. Water molecules 1 and 11 are connected to the ectoplasm and cytoplasm, respectively. All other water molecules are connected only to their neighboring water molecules.

TABLE 1: Comparison of the Experimentally and Computationally (DMC) Determined Proton Flux through the gA Channel for Different pH Values and Membrane Potentials[a]

	Proton Flux [pA]							
	pH 0		pH 0.3		pH 2		pH 2.3	
membrane potential [mV]	exp[b]	DMC	exp[c]	DMC	exp[d]	DMC	exp[e]	DMC
0	2	0 ± 1	0	1 ± 1	0.4	0.0 ± 0.2	−0.05	0.0 ± 0.1
−50	22	3 ± 1	8	4 ± 1	0.7	0.1 ± 0.2	0.42	0.2 ± 0.2
−100	42	7 ± 1	21	8 ± 2	0.9	0.6 ± 0.5	0.71	0.3 ± 0.2
−150	63	14 ± 2	34	15 ± 2	1.1	1.3 ± 0.5	*f*	0.6 ± 0.4
−200	79	23 ± 2	*f*	25 ± 3	1.1	1.9 ± 0.9	*f*	1.1 ± 0.6
−300	105	50 ± 3	*f*	47 ± 3	*f*	4.1 ± 1.1	*f*	2.3 ± 0.7
−400	120	76 ± 5	*f*	69 ± 5	*f*	8.3 ± 1.4	*f*	5.7 ± 1.6
−500	*f*	110 ± 7	*f*	97 ± 4	*f*	13.3 ± 1.3	*f*	7.8 ± 1.4

[a] Experimental data were obtained from published diagrams using the program g3data. Error values given for the DMC calculations are calculated as standard deviations of twenty independently simluated trajectories. [b] Reference 23. [c] Reference 24. [d] Reference 25. [e] Reference 26. [f] Not determined.

For each DMC simulation, 20 trajectories are generated. Since the initial state is set arbitrarily, the system is simulated for 10 000 Monte Carlo steps so that the system can adopt a steady state. The final state of this short simulation is than used as starting configuration of a production run of 5×10^6 Monte Carlo steps. Properties are calculated as average over these 20 trajectories.

Results and Discussion

In this article, we combine a microstate formalism that describes charge transfer reactions[14,15] and a sequential DMC algorithm to simulate the kinetics of long-range proton transfer processes. Energetic parameters of this reaction system are obtained from continuum electrostatic calculations. We present simulations of the proton transfer through gramicidin A (gA) in dependence on external pH and membrane potential. The proton flux obtained by these simulations agrees with experimental values.[23−26]

Energy Profile of the Proton Channel. In order to analyze the proton transfer process within the channel, it is instructive to calculate first the energy profile along the proton transfer path. For this purpose, we computed the potential of mean force (PMF) of the gramicidin A channel for having one or two protons inside the channel. Since in our system only microstates with one or two protons in the channel are significantly populated, all relevant states are considered in the two-dimensional energy profile shown in Figure 5a. Due to the moderate size of our system, the partition function of the system with a limited number of protons in the channel can be calculated and thus the PMF can be obtained from the following two equations (given here for one proton in the channel):

$$\langle u_i \rangle = \frac{\sum_{\nu=1}^{M} u_i \cdot \mathrm{e}^{-G_\nu/RT}}{Z} \tag{17}$$

$$G_{\mathrm{pmf}} = RT \ln\left(\frac{\langle u_i \rangle}{1 - \langle u_i \rangle}\right) \tag{18}$$

$\langle u_i \rangle$ is the probability that the proton is on site i, u_i, is 1 or 0 depending on whether site i is protonated or deprotonated, respectively. Z is the partition function, R is the ideal gas constant, and T is the absolute temperature. The one-dimensional PMF obtained from eq 18 is plotted in Figure 5b (solid line). For a system with one proton in the channel, the minimum energy profile is shown as dashed line. An energy barrier for the charge transfer from one side of the channel to the other is located at the central three water molecules. This energy barrier is about 3.4 kcal/mol if calculated from the PMF profile and 4.6 kcal/mol if calculated from the minimum energy profile. The difference between the minimum energy profile and the PMF profile are entropic contributions due to water molecule rotation, which are taken into account in the PMF profile but not in the minimum energy profile. These entropic contributions lower the energy barrier by about 1.2 kcal/mol. For a one barrier process, such a lowering corresponds to an increase of the overall rate constant by about 1 order of magnitude, which underlines the importance of water rotations in the gA channel. The energy barrier obtained from the PMF is in good agreement with an earlier empirical valence bond calculation.[4]

From the two-dimensional PMF in Figure 5a, one can derive the localization of the protons inside the channel. The lowest energy states are found on the diagonal. This diagonal represents the states with one proton bound. All other states have two protons bound. Low energy states with two protons bound are those in which the protons are on opposite sides of the barrier, i.e., one proton is on water molecule 1 to 4 and the other one is on water molecule 8 to 11.

Proton Flux Through Gramicidin A. In order to compare our sequential DMC calculations with experimental data, the system was simulated at pH values of 0.0, 0.3, 2.0, and 2.3. For each pH value, the proton flux was calculated for membrane potentials ranging from 0 to −500 mV. A trajectory of 8 μs took about 5 min on an Intel Pentium 4 with 3.2 GHz.

Table 1 shows a comparison of the calculated proton flux with experimental data of several groups.[23−26] We obtained an agreement between theory and experiment within 1 order of magnitude with a slight trend of underestimating the proton flux. The calculated proton flux deviates from the experimental value normally only by a factor of 2. We are not only able to reproduce the dependence of the experimental fluxes on the membrane potential at a given pH value, but our simulations also reproduce the increase of the proton flux when the pH is lowered from 2.3 to 0.0. Especially at pH = 0, the discrepancy between theory and experiments is larger. Under these conditions, the model is also expected to describe the real system less satisfactorily, since the pH contributes considerably to the ionic strength at this pH, which is not considered in our calculations. Since in our calculations no other parameters than the pH value and the membrane potential are changed, our model describes correctly the behavior of LRPT in gA over a wide range of pH values and membrane potentials.

TABLE 2: Probability for a Proton Being Transferred from the Ectoplasm to the Cytoplasm[a]

	Proton Transfer Probability [%]					
	number of protons not limited			number of protons limited to one		
water molecule	−100 mV	−300 mV	−500 mV	−100 mV	−300 mV	−500 mV
1	9	37	53	16	62	88
2	9	37	54	16	62	88
3	16	66	82	16	63	88
4	25	83	95	27	75	92
5	37	95	99	52	94	99
6	44	95	99	55	95	99
7	68	97	99	70	97	99
8	92	99	100	90	99	100
9	98	99	100	97	99	100
10	99	99	100	98	99	100
11	99	100	100	99	100	100

[a] All values are calculated at pH = 0. A transfer probability of 68% for water molecule 7 at −100 mV means that 68% of the protons which reached water molecule 7 were transferred across the whole channel afterwards. Columns 2−4 present transfer probabilities of protons if the simulation is not limited to a certain number of protons. Columns 5−7 show the transfer probabilities if the number of protons inside the channel is limited to one.

Proton Transfer Mechanism. The good agreement of the proton flux with experimental values allows to further investigate the mechanism of the LRPT in gA. In the first subsection, we analyze the overall behavior of protons in the gA channel by determining the transfer probability of individual protons. Our sequential DMC approach enables us to follow single protons in the gA channel. Such an analysis is shown in the second subsection. In the last subsection, we will address the question whether the reorientation of the hydrogen bonded network or the electrostatic barrier for the charge transfer is rate limiting for the LRPT process in gA.

Proton Transfer Probability. Table 2 presents the probability that a proton is transferred through the whole channel after reaching a given water molecule. For example, a probability of 68% for water molecule 7 at a membrane potential of −100 mV means that 68% of the protons which reached water molecule 7 after being taken up from the ectoplasmic site are released on the cytoplasmic site. The remaining 32% of protons are returned to the ectoplasmic site. At low membrane potentials (−100 mV) only 9% of the protons that are taken up are transferred across the membrane (see Table 2). The remaining 91% of the protons are released on the same side of the membrane where they entered the channel. But already at this membrane potential, it is obvious from the transfer probabilities that once the proton crosses the central energy barrier, it is most likely transferred across the whole channel. At a membrane potential of −100 mV, once the proton at water molecule 1 has reached water molecule 8, the probability of leaving the channel from water molecule 11 is above 90%. With increasing membrane potential, the proton transfer probabilities increase for all water molecules. Interestingly, for membrane potentials as negative as −300 mV, the first water molecule for which more than 50% of the protons are transferred, is located in front of the energy barrier. Under these conditions, the energy barrier is already greatly diminished, nevertheless a small barrier remains. However, proton transfer through gA is a nonequilibrium process. Thus, discussing transfer probabilities solely on the basis of an energy profile can be misleading.

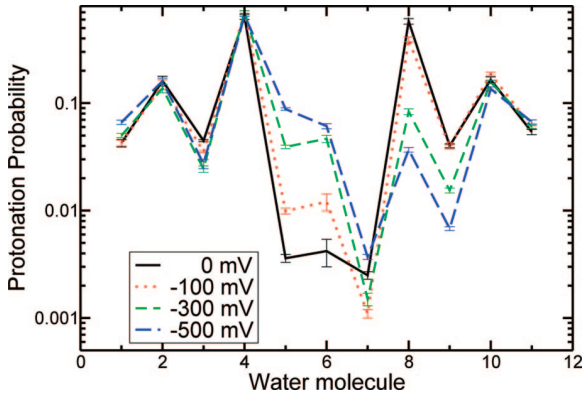

Figure 6. Protonation probability under steady state conditions at membrane potentials of 0, −100, −300, and −500 mV. The overall number of protons in the channel decreases with increasing membrane potential.

Figure 6 shows the protonation probability at pH = 0 of all water molecules at equilibrium conditions (without membrane potential) and at steady state conditions with different membrane potentials. The protonation probabilities of the three central water molecules are very much influenced by the membrane potential. Figure 6 shows that with increasing membrane potential, the protonation probabilities of the water molecules 5 and 6 increases strongly. In contrast, the protonation probabilities of water molecules 8 and 9 decrease with increasing membrane potential. This decrease also leads to an overall reduction of the average number of protons inside the channel from 1.7 (at a membrane potential of 0 mV) to 1.3 (at a membrane potential of −500 mV). The observed shifts of the protonation probabilities under the influence of the membrane potential can be interpreted as follows: Under the influence of the membrane potential, the proton reaches the barrier at the central three water molecules more frequently. Once the barrier is crossed, the proton tends to leave the channel more rapidly the stronger the membrane potential. Nevertheless, the energy profile that could be extracted from the protonation probabilities does not simply contain the membrane potential as an additive contribution, because the protons that crossed the barrier are eventually removed from the channel and thus the steady state protonation differs from an equilibrium protonation.

Analysis of Single Protons in the Channel. Our sequential DMC approach allows to analyze the simulation in analogy to single molecule experiments. We can for instance follow single protons inside the channel. Figure 7 shows such an analysis at different membrane potentials. At a membrane potential of −100 mV (Figure 7a), protons that entered the channel stay on the same site of the channel and are only rarely transferred across the central barrier. The protons enter from both sites and only reach water molecule 4 or 8, depending on the site from which they have entered the channel. This observation correlates with a very low transfer probability of only about 9% for −100 mV. At a membrane potential of −300 and −500 mV, more protons are transferred across the membrane. The actual crossing event is rather fast for all membrane potentials, reflecting the high protonation energies of the central three water molecules. The increase of the number of transferred protons is due to a decrease of the time span a proton stays in front of the barrier. Moreover, the protons also leave the channel faster. If the proton has crossed the barrier, it is generally released. The probability that the proton is crossing the barrier again in the opposite direction is negligibly small. Table 3 shows the average occupation times, i.e., the average time a single proton stays on a water molecule

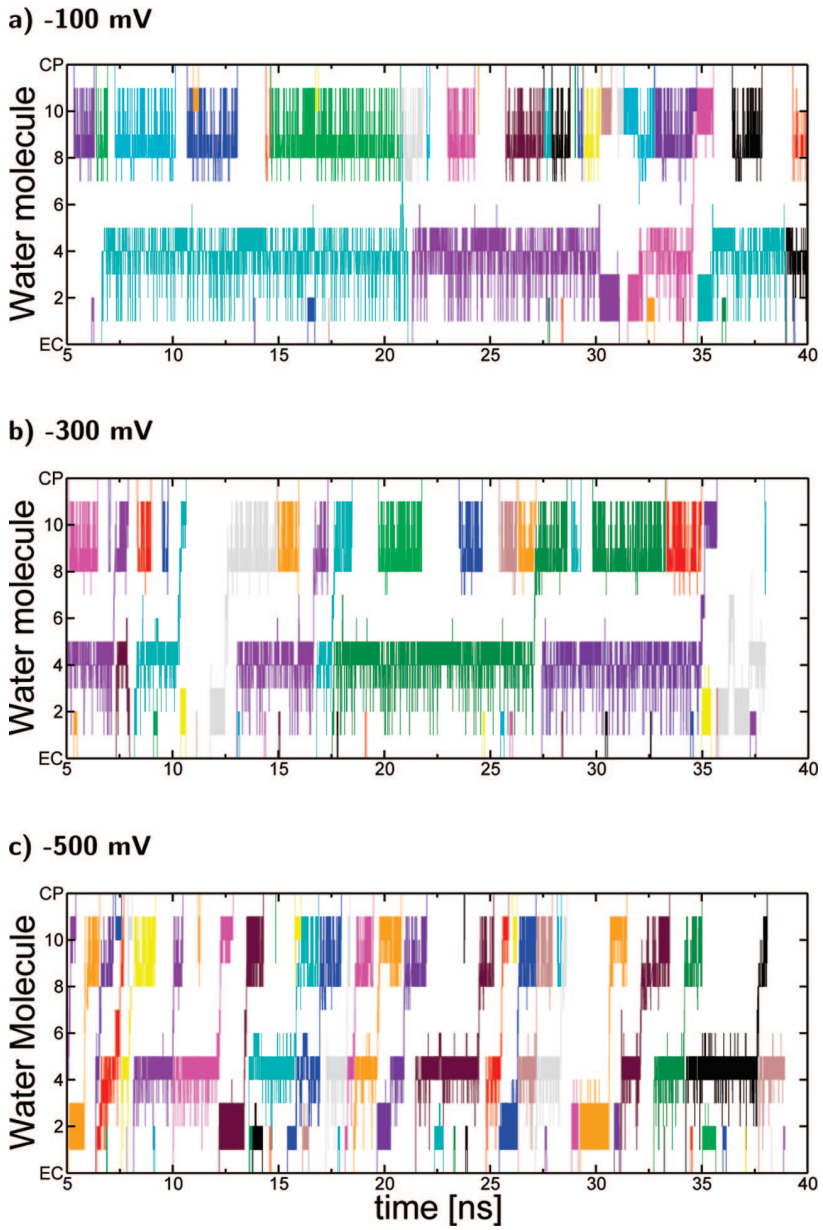

Figure 7. Sections of sequential DMC trajectories, which allow us to follow protons through the gA channel. The diagrams show the location of protons within the first 40 ns of our simulations for membrane potentials of (a) −100, (b) −300, and (c) −500 mV. The colors represent different protons. All simulations are performed at pH = 0.

while it is inside the channel. The proton stays most of the time at water molecules 4 and 8. The actual transfer over the barrier is fast.

As can be seen from Figure 7, there is typically more than one proton inside the channel, i.e., once a proton has crossed the central barrier, the next proton already enters the channel. One thus may ask whether the transfers of these protons are correlated with each other. Therefore, in a second set of simulations, the number of protons inside the channel is limited to one. In these simulations, uptake events are only allowed if no proton is inside the channel. If there is a correlation between two protons inside the channel, the limitation to one proton should result in different transfer probabilities and occupation times. Table 2 shows the transfer probabilities for each water molecule for simulations with an arbitrary number of protons inside the channel and simulations limited to one proton inside the channel. In Table 3, the occupation times of a proton are listed for each water molecule determined from these two sets of simulations. The transfer probabilities shown in Table 2 for the simulations with a limited number of protons increase for the first two water molecules. The changed transfer probabilities indicate that the first proton hinders the second proton from crossing the barrier. This hindrance is due to electrostatic interactions as can be seen from the two-dimensional potential of mean force (Figure 5a). Microstates with two protons close to each other (less than three water molecules distance) have a significantly higher energy than microstates with protons separated by more than three water molecules.

The same picture can be obtained by comparing the occupation times in the simulations with a limited number of protons to the occupation times in the simulations without this limitation. The proton stays much longer on water molecule 4 if there is more than one proton allowed in the channel, but the occupation time for water molecule 8 is similar or even decreased. The first proton, which is on the other side of the barrier, hinders

TABLE 3: Average Occupation Times for All Water Molecules[a]

	Average Occupation Times [ps]					
	number of protons limited to one			number of protons not limited		
water molecules	−100 mV	−300 mV	−500 mV	−100 mV	−300 mV	−500 mV
1	93 ± 7	51 ± 3	23 ± 6	90 ± 4	62 ± 2	51 ± 2
2	491 ± 37	335 ± 24	194 ± 52	316 ± 22	172 ± 14	124 ± 8
3	59 ± 5	62 ± 4	53 ± 12	127 ± 16	53 ± 3	32 ± 3
4	1313 ± 261	1348 ± 132	900 ± 206	3973 ± 545	1953 ± 164	905 ± 49
5	64 ± 12	87 ± 8	99 ± 21	80 ± 9	122 ± 8	125 ± 5
6	109 ± 20	136 ± 9	91 ± 11	103 ± 18	148 ± 9	87 ± 4
7	14 ± 3	5 ± 0	4 ± 1	3 ± 0	4 ± 0	5 ± 0
8	935 ± 225	318 ± 27	76 ± 12	1011 ± 61	143 ± 8	46 ± 2
9	27 ± 5	26 ± 2	10 ± 2	77 ± 6	24 ± 1	8 ± 0
10	325 ± 30	242 ± 15	178 ± 24	330 ± 15	240 ± 10	163 ± 5
11	105 ± 9	91 ± 5	81 ± 11	106 ± 4	91 ± 4	80 ± 3

[a] An occupation time is the total time a single proton stays on a water molecule while it is inside the channel. Columns 2−4 present transfer probabilities of protons if the simulation is not limited to a certain number of protons. Columns 5−7 show the transfer probabilities if the number of protons inside the channel is limited to one. Error values given for the DMC calculations are calculated as standard deviations of 20 independently simluated trajectories.

TABLE 4: Proton Flux through the gA Channel in Dependence on the Membrane Potential for Differently Lowered Electrostatic Barriers and Increased Rotation Rates[a]

	Proton Flux [pA]						
		lowering of the electrostatic energy barrier[b]			factor for rotation rate increase[c]		
membrane potential [mV]	reference flux	−1.0	−2.0	−3.0	5	10	100
0	0 ± 1	2 ± 2	7 ± 3	10 ± 2	2 ± 4	3 ± 5	4 ± 8
−50	3 ± 1	8 ± 2	35 ± 3	42 ± 3	9 ± 3	14 ± 8	30 ± 11
−100	7 ± 1	19 ± 2	62 ± 5	73 ± 3	23 ± 5	30 ± 9	71 ± 15
−150	14 ± 2	32 ± 2	84 ± 4	101 ± 4	41 ± 7	56 ± 13	128 ± 19
−200	23 ± 2	46 ± 4	106 ± 5	131 ± 4	70 ± 9	96 ± 14	184 ± 14
−300	50 ± 3	87 ± 4	146 ± 5	186 ± 4	136 ± 8	177 ± 20	332 ± 24
−400	76 ± 5	129 ± 5	189 ± 4	245 ± 4	208 ± 13	276 ± 21	488 ± 19
−500	110 ± 7	181 ± 5	236 ± 7	316 ± 5	298 ± 12	369 ± 25	625 ± 26

[a] All values are derived at pH = 0. Error values given for the DMC calculations are calculated as standard deviations of twenty independently simluated trajectories. [b] Intrinsic energies of the three central water molecules was lowered by 1, 2, and 3 kcal/mol. [c] The rotation rate is increased by multiplying $A_{\nu\mu}$ in eq 11 by 5, 10, and 100.

the second proton from crossing. The second proton has to stay in front of the barrier until the first proton has left the channel.

These findings indicate a strong correlation between the protons transferred through the gA channel at low pH when on average more than one proton is in the channel. At higher pH values, less protons are in the channel. At pH = 2.3 for instance, on average only 0.1 protons are found in the channel. Under these circumstances, the proton−proton interaction has nearly no influence on the proton flux.

Rate Limiting Step of the LRPT. The rate limiting step of the LRPT in gA is under ongoing discussion.[4,50,51] Two different aspects of the transfer process might be rate limiting. On one hand, protons have to overcome an electrostatic energy barrier to cross the channel;[4] on the other hand, the hydrogen bonded network has to rearrange to allow the next transfer. In order to address the question which aspect is rate limiting, we artificially reduce the electrostatic energy barrier of the LRPT process in gA as well as increase the rotation rates in our simulations. For comparison, it is instructive to describe the LRPT as an one barrier process. Assuming Arrhenius behavior, a decrease of the energy barrier by 1.0 kcal/mol increases the transfer rate by a factor of 5, a decrease by 1.35 kcal/mol increases the transfer rate by a factor of 10 and a decrease by 2.7 kcal/mol increases the rate by a factor of 100. In our simulations, the energy barrier is reduced by lowering the intrinsic energies ($G_{\mathrm{intr}}(x_i)$ in eq 1) of the protonated forms of the central three water molecules by 1, 2, or 3 kcal/mol. The rotation rates are increased by multiplying the preexponential factor ($A_{\nu\mu}$ in eq 11) by 5, 10, or 100. If the electrostatic energy barrier is the rate limiting step of the LRPT, the reduction of this barrier should result in a higher proton flux through the gA channel. If the rearrangement of the hydrogen bonded network is rate limiting, the increased rotation rate should increase the proton flux. As can be seen from Table 4, lowering the electrostatic barrier has a significant effect on the observed proton flux. At a membrane potential of −100 mV, decreasing the barrier by 3 kcal/mol increases the flux about 10-fold. And even at membrane potentials as negative as −500 mV, we still observe an increase of the flux from 110 to 316 pA.

Increasing rotation rates also increases the flux. For membrane potentials between 0 and −200 mV, the influence of increasing the rotation rates on the observed flux is similar to the influence of lowering the electrostatic barrier. For membrane potentials more negative than −200 mV, increasing the rotation rates is even more effective than lowering the electrostatic barrier. At a membrane potential of −500 mV, an increase of the rotation rates by a factor of 100 increases the flux from 110 to 625 pA.

The increase of the proton flux by lowering the electrostatic energy barrier is expected to attenuate at higher membrane potentials, since stronger membrane potentials diminish the influence of the electrostatic energy barrier on the LRPT process. The increase of the proton flux by increasing the rotation rates is not influenced by stronger membrane potentials. At small membrane potentials between 0 and −200 mV both the

electrostatic energy barrier and the rotations of the participating molecules similarly influence the LRPT in gA. An increased flux can be achieved both by lowering the electrostatic energy barrier as well as by increasing the rotation rates of the participating molecules.

Conclusions

In this work, we introduce a sequential dynamical Monte Carlo algorithm to simulate long-range proton transfer processes in biomolecules on timescales which are not accessible by other methods up to now. This algorithm allows us to simulate proton transfer processes in dependence on external parameters. We applied the new method to simulate the proton flux through gramicidin A as a function of pH and membrane potential. The calculated proton flux agrees well with experimental data, which gives us confidence to investigate the underlying proton transfer mechanism. In contrast to conventional dynamical Monte Carlo, the new method allows us to analyze our simulation in analogy to single molecule experiments. From this analysis, it can be seen that the proton can only cross the barrier, when the previously transferred proton has already left the channel. Thus at low pH, proton−proton interaction inside the channel is an important factor influencing the proton transfer through gramicidin A. By varying the electrostatic barrier for the proton transfer and the rotation rates of the water molecules, we analyzed the rate limiting process of the proton transfer through gramicidin A. We conclude that at physiological membrane potentials, i.e., between 0 and −250 mV, both aspects of the long-range proton transfer in gramicidin A, the electrostatic barrier and the reorientation of the hydrogen bonded network, are equally important.

By analyzing the proton transfer process, we could show that at low pH a proton which has entered the channel has to wait in front of the electrostatic energy barrier as long as a second proton is still in the channel. Once the proton has crossed the electrostatic energy barrier, it is transferred across the whole membrane with a probability of more than 90%.

The new sequential DMC algorithm can be applied to other proteins that are involved in charge transfer. The method can be straightforwardly extended to include electron transfer and coupled proton/electron transfer. It will allow to analyze the detailed mechanism of coupled charge transfer reactions in proteins on biologically relevant time scales.

Acknowledgment. This work was supported by the Deutsche Forschungsgemeinschaft (UL 174/7-1 and UL 174/4-3). We thank Donald Bashford for providing his program MEAD. R. Thomas Ullmann assisted us in designing the water model.

References and Notes

(1) Krishtalik, L. I. *Biochim. Biophys. Acta* **2000**, *1458*, 6–27.
(2) Nagle, J. F.; Morowitz, H. J. *Proc. Natl. Acad. Sci. U.S.A.* **1978**, *75*, 298–302.
(3) Agmon, N. *Chem. Phys. Lett.* **1995**, *244*, 456–462.
(4) Braun-Sand, S.; Burykin, A.; Chu, Z. T.; Warshel, A. *J. Phys. Chem. B* **2005**, *109*, 583–592.
(5) Warshel, A. *Acc. Chem. Res.* **2002**, *35*, 385–395.
(6) Warshel, A. *Chem. Rev.* **1993**, *93*, 2523–2544.
(7) Voth, G. A. *Acc. Chem. Res.* **2006**, *39*, 143–150.
(8) Braun-Sand, S.; Strajbl, M.; Warshel, A. *Biophys. J.* **2004**, *87*, 2221–2239.
(9) Warshel, A.; Weiss, R. M. *J. Am. Chem. Soc.* **1980**, *102*, 6218–6226.
(10) Schmitt, U. W.; Voth, G. A. *J. Chem. Phys.* **1999**, *111*, 9361–9381.
(11) Friedman, R.; Nachliel, E.; Gutman, M. *Biochim. Biophys. Acta* **2005**, *1710*, 67–77.
(12) Marx, D. *Com. Phys. Commun.* **2006**, *7*, 1848–1870.
(13) Lill, M. A.; Helms, V. *J. Chem. Phys.* **2001**, *115*, 7993–8005.
(14) Ferreira, A.; Bashford, D. *J. Am. Chem. Soc.* **2006**, *128*, 16778–16790.
(15) Becker, T.; Ullmann, R. T.; Ullmann, G. M. *J. Phys. Chem. B* **2007**, *111*, 2957–2968.
(16) Gillespie, D. T. *J. Phys. Chem.* **1977**, *81*, 2340–2361.
(17) Fichthorn, K. A.; Weinberg, W. H. *J. Chem. Phys.* **1991**, *95*, 1090–1096.
(18) Burkhart, B. M.; Li, N.; Langs, D. A.; Pangborn, W. A.; Duax, W. L. *Proc. Natl. Acad. Sci. U.S.A.* **1998**, *95*, 12950–12955.
(19) Eisenman, G.; Enos, B.; Hagglund, J.; Sandblom, J. *Ann. N.Y. Acad. Sci.* **1980**, *339*, 8–20.
(20) Andersen, O. S.; Koeppe, R. E.; B, R. *IEEE Trans. Nanobiosci.* **2005**, *4*, 10–20.
(21) Pomes, R.; Roux, B. *Biophys. J.* **2002**, *82*, 2304–2316.
(22) de Groot, B. L.; Tieleman, D. P.; Pohl, P.; Grubmüller, H. *Biophys. J.* **2002**, *82*, 2934–2942.
(23) Chernyshev, A.; Cukierman, S. *Biophys. J.* **2006**, *91*, 580–587.
(24) Cukierman, S. *Biophys. J.* **2000**, *78*, 1825–1834.
(25) Akeson, M.; Deamer, D. W. *Biophys. J.* **1991**, *60*, 101–109.
(26) Cukierman, S.; Quigley, E. P.; Crumrine, D. S. *Biophys. J.* **1997**, *73*, 2489–2502.
(27) Homeyer, N.; Essigke, T.; Ullmann, G.; Sticht, H. *Biochemistry* **2007**, *46*, 12314–12326.
(28) Klingen, A. R.; Bombarda, E.; Ullmann, G. M. *Photochem. Photobiol. Sci.* **2006**, *5*, 588–596.
(29) Ullmann, G. *J. Phys. Chem. B* **2003**, *107*, 1263–1271.
(30) Ullmann, G. M.; Knapp, E.-W. *Eur. Biophys. J.* **1999**, *28*, 533–551.
(31) Bombarda, E.; Becker, T.; Ullmann, G. M. *J. Am. Chem. Soc.* **2006**, *128*, 12129–12139.
(32) Landau, D. P.; Binder, K. *A Guide to Monte Carlo Simulations in Statistical Physics*; Cambridge University Press: New York, 2000.
(33) Prados, A.; Brey, J.; SanchezRey, B. *J. Stat. Phys.* **1997**, *89*, 709–734.
(34) Sadhukhan, S.; Munoz, D.; Adamo, C.; Scuseria, G. E. *Chem. Phys. Lett.* **1999**, *306*, 83–87.
(35) Pavese, M.; Chawla, S.; Lu, D. S.; Lobaugh, J.; Voth, G. A. *J. Chem. Phys.* **1997**, *107*, 7428–7432.
(36) Lill, M. A.; Helms, V. *J. Chem. Phys.* **2001**, *115*, 7985–7992.
(37) Barroso, M.; Arnaut, L. G.; Formosinho, S. J. *J. Phys. Chem. A* **2007**, *111*, 591–602.
(38) Cherepanov, D. A.; Junge, W.; Mulkidjanian, A. Y. *Biophys. J.* **2004**, *86*, 665–680.
(39) Mulkidjanian, A. Y.; Heberle, J.; Cherepanov, D. A. *Biochim. Biophys. Acta* **2006**, *1757*, 913–930.
(40) Espinosa, E.; Molins, E.; Lecomte, C. *Chem. Phys. Lett.* **1998**, *285*, 170–173.
(41) Woutersen, S.; Emmerichs, U.; Bakker, H. J. *Science* **1997**, *278* (5338), 658–660.
(42) Townsley, L. E.; Tucker, A, W.; Sham, S.; Hinton, F, J. *Biochemistry* **2001**, *40*, 11676–11686.
(43) Brooks, B. R.; Bruccoleri, R. E.; Olafson, B. D.; States, D. J.; Swaminatha, S.; Karplus, M. *J. Comput. Chem.* **1983**, *4*, 187–217.
(44) Swart, M.; Van Duijnen, P. T.; Snijders, J. G. *J. Chem. Phys.* **2001**, *22*, 79–88.
(45) Guerra, C. F.; Snijders, J. G.; te Velde, G.; Baerends, E. J. *Theor. Chem. Acc.* **1998**, *99*, 391–403.
(46) Bashford, D.; Gerwert, K. *J. Mol. Biol.* **1992**, *224*, 473–486.
(47) MacKerell, A. D.; Bashford, D.; Bellott, M.; Dunbrack, R. L.; Evanseck, J. D.; Field, M. J.; Fischer, S.; Gao, J.; Guo, H.; Ha, S.; Joseph-McCarthy, D.; Kuchnir, L.; Kuczera, K.; Lau, F. T. K.; Mattos, C.; Michnick, S.; Ngo, T.; Nguyen, D. T.; Prodhom, B.; Reiher, W. E.; Roux, B.; Schlenkrich, M.; Smith, J. C.; Stote, R.; Straub, J.; Watanabe, M.; Wiorkiewicz-Kuczera, J.; Yin, D.; Karplus, M. *J. Phys. Chem. B* **1998**, *102*, 3586–3616.
(48) Im, W.; Beglov, D.; Roux, B. *Com. Phys. Commun.* **1998**, *111*, 59–75.
(49) Roux, B. *Biophys. J.* **1997**, *73*, 2980–2989.
(50) de Groot, B. L.; Frigato, T.; Helms, V.; Grubmüller, H. *J. Mol. Biol.* **2003**, *333*, 279–293.
(51) Jensen, M. O.; Tajkhorshid, E.; Schulten, K. *Biophys. J.* **2003**, *85*, 2884–2899.

JP801477B